J. Phys. D: Appl. Phys. **41** (2008) 024001 (11pp) doi:10.1088/0022-3727/41/2/024001

Fast (tens to hundreds of eV) neutral beams for materials processing

Demetre J Economou

Plasma Processing Laboratory, Department of Chemical and Biomolecular Engineering, University of Houston, Houston, TX 77204-4004, USA

E-mail: economou@uh.edu

Received 1 June 2007, in final form 21 August 2007
Published 4 January 2008
Online at stacks.iop.org/JPhysD/41/024001

Abstract

Fast neutral beams (beam energy of tens to hundreds of eV) may be useful for mitigating charging damage that can occur in conventional plasma processing of materials. For neutral beam processing to be viable, however, the beam energy, flux and directionality must be comparable to those in traditional reactive ion etching or reactive ion beam technologies. This paper provides a review of fast neutral beams for materials processing. Neutral beam generation techniques are outlined. Characterization of neutral beams is important to measure the beam flux, energy and angular distributions. Neutral beam materials processing is discussed with emphasis on etching of thin films.

1. Introduction

Plasma processing is critical for fabricating microelectronic circuits [1]. In plasma etching, a solid film on a wafer surface turns into a volatile product when exposed to a reactive gas plasma. Reaction on the surface occurs by simultaneous bombardment of the film by energetic positive ions and (thermal energy) neutrals. In plasma deposition, a film grows on the wafer surface exposed to a reactive plasma. In both cases, the wafer is also exposed to a flux of electrons from the plasma.

In a continuous wave discharge, positive ions bombarding the wafer have a strongly anisotropic velocity distribution, while electrons have an almost isotropic velocity distribution (figure 1). As a result, the bottom of a feature (trench, hole) charges positively, while the sidewalls charge negatively. This differential charging causes positive ions entering the feature to deflect towards the walls, possibly inducing sidewall bow and reducing the ion flux at the bottom [2–4]. The reduction of the ion flux as a function of depth in a feature can lead to aspect ratio dependent etching (ARDE) or even etch stop [5]. Most often the etch rate decreases with increasing aspect ratio (reactive in etching (RIE) lag). It is a very complex process, where, in addition to charging, imperfect collimation of the bombarding ions, depletion of reactant by wall reactions, polymer deposition and redeposition of reaction products may also play a role [6]. The net effect is that small features etch slower than larger ones on the same substrate. In addition to

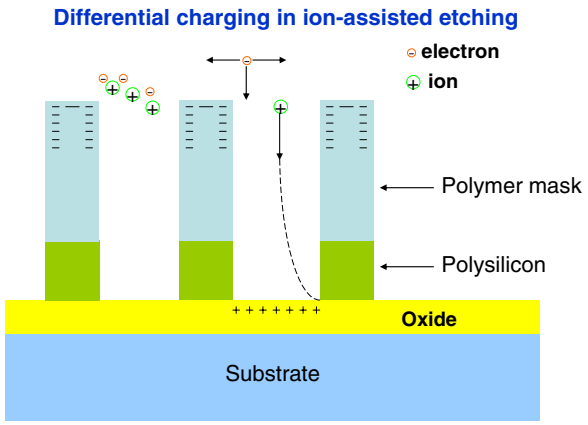

Figure 1. Differential charging of features and deflection of ion trajectories in RIE.

(This figure is in colour only in the electronic version)

the obvious throughput penalty, designing an etching process to accommodate RIE lag requires higher selectivity with respect to masking and etch-stop layers and/or the use of thicker masking layers, all of which add processing cost. The ability to eliminate any one of the contributors to RIE lag, or ARDE in general, would be extremely beneficial. Charging is to be expected when etching polymers, oxide and other dielectrics. It is, however, a far more general concern, because it can occur in any process that uses a resist mask; an example is notching [7,8] on the sidewalls of polysilicon gates. As device

dimensions continue to shrink and feature aspect ratios keep increasing, charging problems are expected to become even more important in the future. Charging of wafers exposed to a plasma can also lead to gate oxide breakdown [9].

Charging artefacts could be reduced or eliminated by using energetic neutral beams (fast atoms or molecules), instead of ions, to give the directional component of reactive etching. For, while surfaces might still charge through secondary electron emission, there would be no effect on the neutral particle trajectories and, hence, no charging contribution to ARDE, sidewall bowing or notching. To be competitive with conventional RIE, neutral beams must have the following characteristics: beam flux (equivalent) greater than $\sim$1 mA cm^{-2} (i.e. 0.62×10^{16} particles cm^{-2} s^{-1}) controllable beam energy for tens to hundreds of eV, high degree of collimation (angular divergence of at most several degrees) and large area coverage (at least 300 mm diameter wafers).

This paper provides a review of fast (kinetic energy of tens to hundreds of eV) neutral beams for materials processing. Neutral beam generation techniques are presented first. Neutral beam materials processing is discussed next with emphasis on etching of thin films. Neutral beam diagnostics to measure the beam flux and energy are also outlined.

The focus of this paper is on neutral beams with kinetic energy greater than $\sim$10 eV. There are numerous works on neutral beams with energy of less than $\sim$10 eV, produced, for example, by supersonic expansion of a heated gas or laser generated plasma, laser vaporization of cryogenic solids, electron stimulated desorption and charge exchange downstream of electron cyclotron resonance (ECR) plasmas (see [10] for a review). Some of the earlier works were motivated by the need to study the interaction of materials exposed to O atoms (energy of several eV) in a low earth orbit (LEO) environment [11].

2. Generation of fast neutral beams

There are two common methods to produce fast neutral beams: volume neutralization and surface neutralization. In both cases, one starts with an ion beam of certain energy and flux. This beam is normally produced using a plasma. In some cases, ions are first extracted from the plasma (for example gridded ion sources) and are then neutralized in the gas phase or on surfaces [12–25]. In other cases, ion extraction and neutralization occur simultaneously using a single grid [26–29].

2.1. Volume neutralization of ions

Volume neutralization is based on charge exchange between the ion beam and a background gas. For example, for an argon ion beam in a background of argon atoms,

$$\mathrm{Ar^+(fast) + Ar(slow) \rightarrow Ar(fast) + Ar^+(slow)}, \qquad (1)$$

whereby a fast (beam) ion is converted to a fast (beam) neutral, and a slow neutral (of the background gas) is converted to a slow ion. Data on the cross section of this process [1, p 77] can be fit to yield $\sigma_{CX} = 47.05(1.0 - 0.0557 \ln \varepsilon)^2$ [30], where σ_{CX} is the charge exchange cross section and ε is the fast ion energy. The cross section for (elastic) scattering is given by $\sigma_{SC} = 40.04(1.0 - 0.0563 \ln \varepsilon)^2$. In these expressions, the cross section comes out in units of 10^{-16} cm^2 when the ion kinetic energy is in eV.

The charge exchange reaction (1) does not change the directionality of the fast ion. Also, resonant charge exchange (between an ion and its parent neutral as shown in reaction (1)) has a cross section which is often one order of magnitude larger than the corresponding non-resonant charge exchange process. However, scattering by (non-charge exchange) collisions can also occur as the ion beam propagates through the neutral background gas. Gas phase scattering can reduce the ion beam flux and directionality and should be minimized. Several researchers have reported on neutral beam sources based on the charge exchange of ions with a background neutral gas [12–16]. However, etch rates were low ($<$10 nm min^{-1}) and there was a trade-off between etch rate and beam collimation. Positive ions are used in the majority of situations. However, negative ions are preferred at high energies ($>$50 keV) because they can be neutralized more efficiently (see section 3.5). Collimated neutral beams formed by volume neutralization should have an energy distribution similar to the parent ion beam.

2.2. Surface neutralization of ions

Surface neutralization is based on the interaction of the ion beam with a solid surface. Ions coming in contact (within $\sim$1 Å) with the surface are, for example, Auger neutralized to form neutrals. The angle of impact of ions on the surface is critical. Ions impacting the surface at large angles with respect to the normal to the surface (e.g. at grazing angles) are more likely to scatter forward [31], and the emerging neutral beam retains more of the directionality of the parent ion beam. In addition, the energy loss of these ions is a small fraction of their initial kinetic energy. For example, a model [32] assuming specular scattering of the projectile off a surface, suffering two successive binary collisions with surface atoms, gives

$$\sqrt{\frac{\varepsilon_r}{\varepsilon_i}} = \left(\frac{\mu}{\mu+1}\right)^2 \left(\cos\chi_{1/2} + \sqrt{\frac{1}{\mu^2} - \sin^2\chi_{1/2}}\right)^2, \qquad \chi_{1/2} = \frac{\pi}{2} - \theta_i, \qquad \mu = \frac{m_{ion}}{m_{wall}}. \qquad (2)$$

Here ε_i and ε_r are kinetic energy of the incident and reflected species, respectively, θ_i is the incident angle (with respect to the surface normal) and m_{ion} and m_{wall} are the mass of the ion and the surface material atom, respectively. This formula predicts an energy loss of $\sim$3 eV for 90 eV argon ions impinging on a silicon surface at $\theta_i = 84^\circ$. Under these conditions, the emerging neutral beam would retain much of the energy of the parent ion beam. In contrast, ions impacting the surface at small angles will scatter more diffusively and will lose a larger fraction of their impact kinetic energy. This is because these ions will penetrate the solid and will have a better chance to closely interact with more atoms, thereby losing more of their initial kinetic energy as well as their sense of direction.

The neutralization of ions by grazing collisions with a metal surface has been studied extensively [33–35]. The collision process is typically modelled in three stages: the initial interaction as the ion approaches the surface, the 'close encounter' where the possibly neutral particle changes direction due to one or more collisions with the nuclei of the atoms on the surface and the final interaction as it moves away [36]. Studies on amorphous [37] as well as single crystal scattering surfaces [38] have shown that the initial charge state of the projectile (positive, negative, or neutral) has no influence on the charge state of the particle that finally emerges from the collision. In other words, memory of the initial charge state is lost during the close encounter with the metal surface. While the extensive ion scattering experiments carried out in the past have led to much understanding of the interaction between charged particles and clean surfaces [39], the link between fundamental mechanisms and the scattering of ions from the rough, practical surfaces, possibly contaminated by etching species as well as etching by-products that are encountered in a neutral beam source, is difficult to make.

Goeckner *et al* [17] and Nichols and Manos [21] produced a neutral beam by reflecting accelerated ions off a metal surface at an angle with the ion beam. The resulting neutral flux was relatively low. In addition, in the case of non-grazing angle collisions, there is concern of contamination by the sputtered material from the neutralizing surface. Eipers-Smith *et al* [22] and Lu and co-workers [23, 24] used a Kaufman-type ion source to generate an ion beam that was neutralized with a conical nickel neutralizer. This neutralizer acted as a 'funnel' giving the resulting neutral beam a geometric focus on the substrate thereby enhancing the fast neutral flux. However, this configuration is not suitable for processing large area wafers. Chen and Yang [25] used a grid to extract positive ions out of an inductively coupled plasma (ICP) source. A second grid was used to neutralize these ions before interacting with a wafer downstream. Kim *et al* [20] produced a fast neutral beam by extracting ions from an ion source and neutralizing these ions by glancing angle collisions on the surfaces of a set of parallel metal plates.

2.3. Neutral beam sources using simultaneous ion extraction and neutralization

Simultaneous ion extraction and neutralization has the advantage of larger neutral beam flux and better control over beam characteristics. Ions are extracted from a plasma through a high aspect ratio grid and are neutralized during their transit through the holes of the grid. A neutral beam source based on simultaneous ion extraction and neutralization [26] is shown in figure 2. An ICP is ignited in an alumina tube by supplying 13.56 MHz radio frequency (RF) power to a three-turn coil, through a matching network. Ions generated in the plasma are accelerated out of the plasma by a 'beam acceleration electrode' attached to the top of the ICP source. A boundary voltage (V_b) is generated by coupling the beam acceleration electrode to the RF power supply by a variable capacitor (C_b). By changing C_b, the boundary voltage V_b can be varied, which provides control over the ion energy and hence the

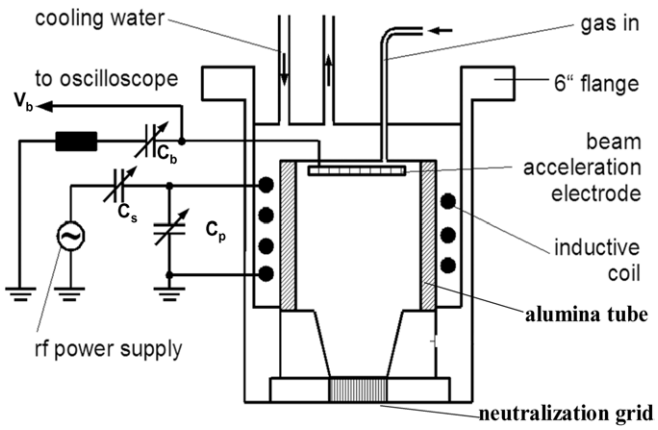

Figure 2. Neutral beam source using a single ion extraction/neutralization grid. (From [26].)

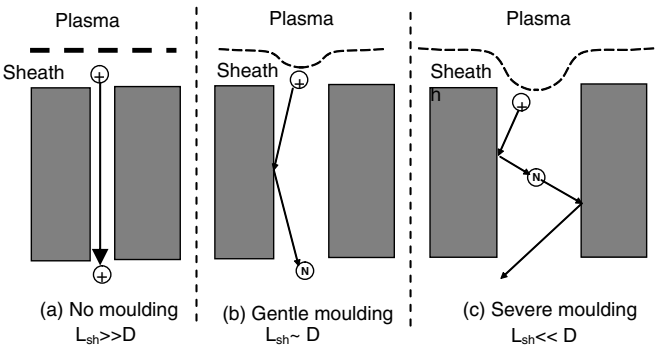

Figure 3. Schematic of ion neutralization by collision on the sidewall of a grid hole. The 'bending' of the plasma–sheath meniscus over the hole (plasma moulding) is also shown. Plasma moulding is absent when the sheath thickness (L_{sh}) is much greater than the hole diameter (D), i.e. $L_{sh} \gg D$. At the other extreme ($L_{sh} \ll D$) plasma moulding is severe.

resulting neutral beam energy (in the range of 20 eV to more than 200 eV). The accelerated ions pass through a grounded neutralizion grid, strike the internal surfaces of the holes of the grid (preferentially at grazing angles) and are converted to fast neutrals (figure 3). Low pressure in the plasma source (large mean free path) minimizes the probability of charge exchange collisions between ions and slow neutrals; thus surface neutralization is dominant. The substrate is placed a small distance downstream of the neutralization grid in a differentially pumped processing chamber (not shown). The pressure in the processing chamber during operation of the source is typically more than 10× smaller than the pressure in the plasma (e.g. 10 mTorr in the plasma and 0.5 mTorr in the processing chamber). Low pressure minimizes gas phase scattering and helps beam collimation and flux. It should be noted that wafer contamination by sputtering of the extraction/neutralization grid should not be an issue in a properly designed neutral beam source. If ions suffer grazing angle collisions with the internal surfaces of the holes, the sputtering yield will be very low. Also, any sputtered material has a high probability to redeposit inside the high aspect ratio holes.

Samukawa *et al* [28,29] also presented a fast neutral beam source based on simultaneous ion extraction and neutralization

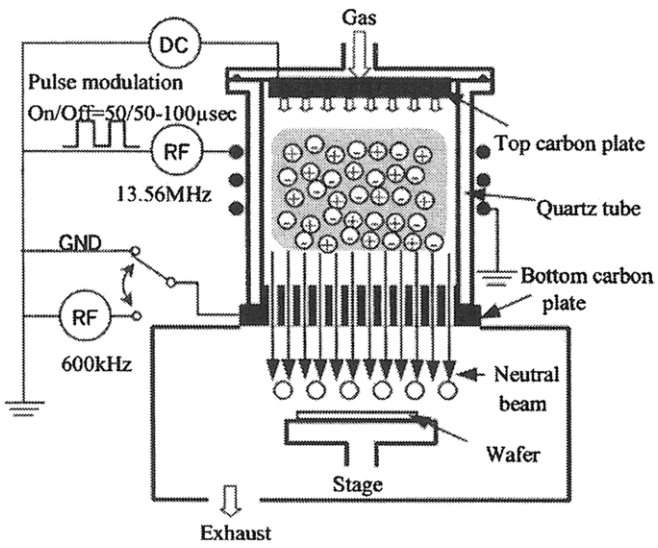

Figure 4. Neutral beam source using a single ion extraction/neutralization (bottom) electrode and a pulsed plasma in electronegative gas. The top or the bottom electrode (or both) may be biased. (From [29].)

through a grid (figure 4). A high density ICP is generated in a quartz tube. A bias is applied to the top carbon electrode in contact with the plasma to push ions through the high aspect ratio holes of the bottom (extraction) carbon electrode. The authors studied neutral beams based on both positive and negative ion extraction and neutralization. To utilize negative ions they used a pulsed discharge in an electronegative gas (Cl_2 or SF_6). In the afterglow of the pulsed discharge, electrons attach to molecules generating negative ions. Provided the afterglow period is long enough, an ion–ion plasma forms [40] and negative ions can be 'pushed out' of the plasma by applying a negative bias to the top electrode. An optional dc or RF (e.g. 600 kHz) bias may also be applied to the bottom (extraction) electrode to provide additional control over the neutral beam energy [41]. The extraction electrode has a high aspect ratio through holes (1 mm diameter and 10 mm long). Negative ions suffer grazing angle collisions with the internal surfaces of the holes turning into fast neutrals. The authors reported that negative ions can be neutralized more efficiently compared with positive ions [29]. It was later conjectured that this is because of differences in the angular distributions of the species (positive versus negative ions) entering the holes [42]. Negative ions enter with a wider angular distribution and are more likely to collide with the sidewall of the holes resulting in greater neutralization efficiency (NE). Charge exchange with neutral gas may also play a role at higher pressures. Besides providing a reasonably high flux and controlled energy, these neutral beam sources [26–29] offer an additional benefit. For example, vacuum ultraviolet (VUV) and ultraviolet (UV) light generated in the plasma is known to cause electrical damage to sensitive devices [43] during conventional plasma processing. However, VUV and UV radiation emanating from the plasma is effectively blocked by the extraction/neutralization grid having high aspect ratio holes, reducing VUV/UV damage to sensitive devices.

2.4. Fundamentals of ion extraction and neutralization through grid holes

The properties (flux, energy, directionality) of neutral beams generated by simultaneous extraction and neutralization of ions through grid holes depend critically on the interaction of the plasma with the holes (plasma moulding). Plasma moulding [44–47] refers to the ability of the plasma–sheath interface to 'contour' along the topography of surface features in contact with the plasma. In the case of plasma in contact with a grid, plasma moulding depends primarily on the diameter of the grid hole, D, as compared with the plasma–sheath thickness, L_{sh}. When $L_{sh} \gg D$, the plasma–sheath interface (meniscus) is essentially planar as if the hole was not there (e.g. a solid wall). In the other extreme, $L_{sh} \ll D$, the plasma 'leaks' through the hole. In the intermediate case, $L_{sh} \sim D$, the plasma–sheath meniscus 'bends' gently over the hole.

Figure 5 shows the time-average potential distribution and the strength of the (time-average) horizontal component of the electric field over a 154 μm diameter hole. These profiles were calculated for a RF plasma discharge in contact with the hole using a self-consistent particle-in-cell (PIC) simulation [48]. Case (a) corresponds to a lower plasma density (thicker sheath) compared with case (b). For a given hole size, plasma moulding is less when the sheath is thicker, yielding weaker lateral electric fields around the hole opening (compare (c) with (d)). Ions entering the hole experience these horizontal fields and are deflected towards the walls. Ion deflection and the angle by which ions strike the wall depend on the severity of plasma moulding.

It appears that there is an optimum 'bending' of the plasma–sheath meniscus over a hole that results in best neutral beam source performance. If the plasma–sheath meniscus is planar (thick sheath, figure 3(*a*)), ions entering the hole are highly directional and pass through the hole without collision with the sidewall. Thus the NE is low, resulting in low neutral beam flux. On the other hand, if the plasma–sheath meniscus dips deep inside the hole (figure 3(*c*)) almost all ions strike the sidewall and neutralize, resulting in higher neutral flux, but worse neutral beam directionality. Also, since ions strike the sidewall at small angles (with respect to the normal on the sidewall), ions lose a larger fraction of their energy, reducing the energy of the fast neutral beam. Under these conditions, fast neutrals may also suffer multiple collisions with the sidewall worsening the situation. Nam *et al* [48] found that optimum neutral beams are extracted by maximizing the number of 'good' ions entering the grid holes. In general, ions that neutralized on the top section of the hole sidewall were 'bad,' in the sense that these ions yielded divergent neutral beams of relatively low energy. Ions that neutralized along the bottom section of the hole sidewall were 'good,' in the sense that these ions yielded neutral beams that were less divergent and retained more of the energy of the parent ions. A three-grid ion extraction/neutralization system was proposed to increase the fraction of good ions and improve the quality of the extracted fast neutral beam. This system allowed plasma moulding to be controlled, even for high plasma densities and large hole diameters, when plasma moulding for a one-grid system would be severe (figure 3(*c*)).

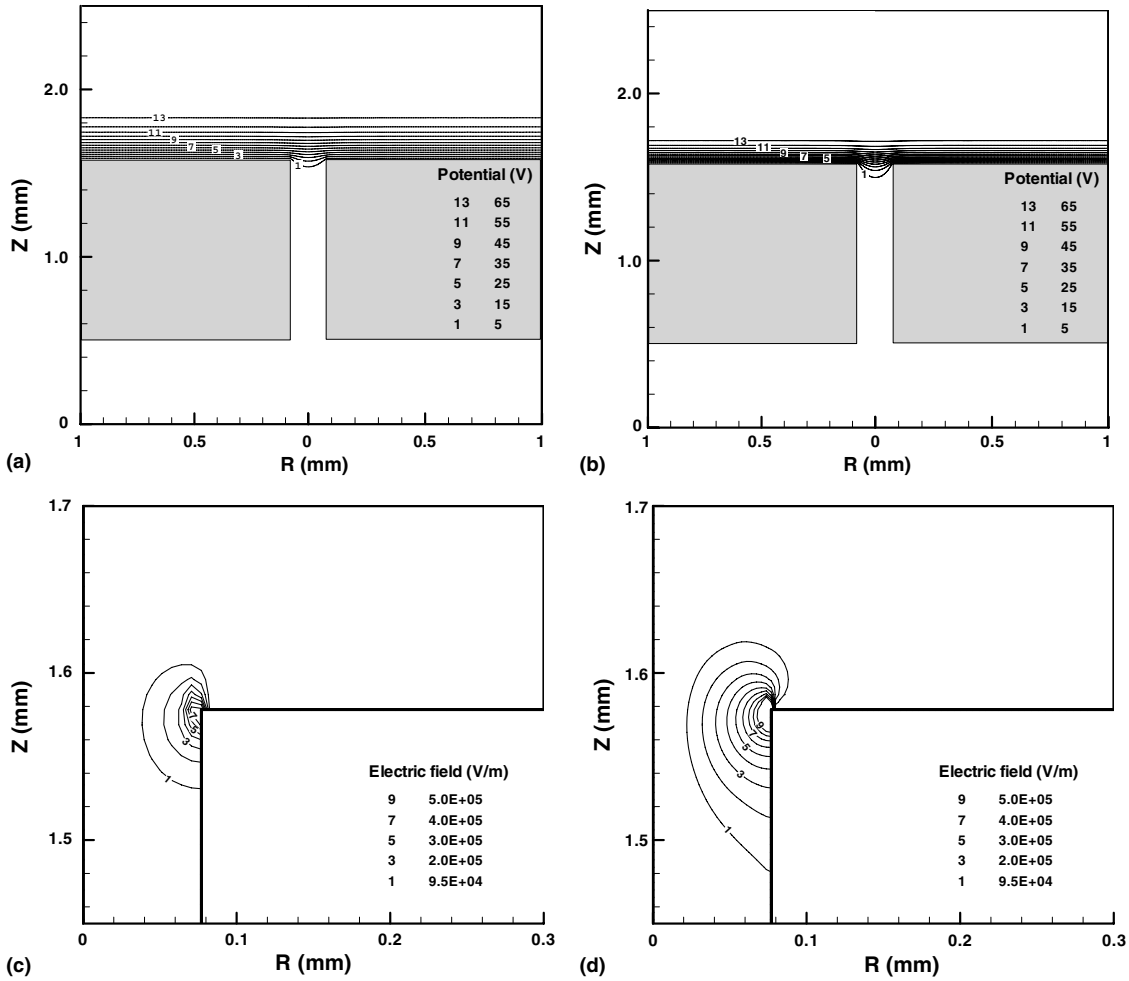

Figure 5. Time-average potential distribution around holes with diameter 154 μm and plasma density of 1×10^{11} cm^{-3} (*a*) and 3×10^{11} cm^{-3} (*b*). Time-average horizontal component of the electric field for plasma density of 1×10^{11} cm^{-3} (*c*) and 3×10^{11} cm^{-3} (*d*). Ion flow was from top to bottom through the hole in a 1078 μm thick solid grid (represented by the gray area). (From [48].)

3. Materials processing using neutral beams

3.1. Thin film etching

Several thin film etching studies using neutral beams have been reported in the literature. Mizutani and Yunogami [12] developed a neutral beam etcher using a Kaufman-type ion source (ion gun) to generate Ar ions in the 200–700 eV range. Charge exchange with the background neutral gas produced an energetic neutral beam. A CHF_3 microwave plasma independently provided neutral (thermal energy) radicals to assist the etching process. The etch rate of SiO_2 with the neutral beam was about 10 nm min^{-1} at 700 eV and this was half of the etch rate obtained with a comparable ion beam. Capacitance–voltage (C–V) measurements showed that there was no reduction in the breakdown voltage (compared with a standard) when the samples were subjected to neutral beam etching. In contrast, breakdown occurred at lower voltages when the samples were subjected to ion beam etching. To overcome the limitation of low etch rates, a co-axial neutral beam assisted etcher was developed [13]. In this configuration, a co-axial discharge tube generated two cylindrical plasmas; the inner one served as the neutral beam source and the outer one served as the (thermal) neutral radical source. A 500 eV Ar neutral beam gave a maximum etch rate of 60 nm min^{-1} for SiO_2. To overcome the limitation of the lack of etch uniformity obtained with the co-axial etcher, a tandem neutral beam etcher was further developed [14], where the neutral beam source and the (thermal) neutral radical source were arranged in tandem. Highly anisotropic and uniform etching was obtained, but the maximum SiO_2 etch rate was still only 76 nm min^{-1}.

Using the charge exchange mechanism, a low energy (10–20 eV) neutral stream of chlorine atoms was extracted from an ECR plasma [15, 16]. An etch rate of 10 nm min^{-1} for Si was obtained which was about 10% of that realized with ion stream etching. Goeckner *et al* [17] produced hyperthermal neutrals by accelerating ions to a surface where they were neutralized and reflected. Using an O_2/Ar mixture, they obtained resist etch rates up to 22 nm min^{-1} and a fast neutral flux of about 2×10^{14} cm^{-2} s^{-1}. Shimokawa and co-workers [18, 19] used an ion source to develop a fast-atom-beam (FAB). The beam energy was 1–3 keV and the beam current was 0.1–1 mA cm^{-2}, with about 95% neutralization. Resist etch rates of 300–500 nm min^{-1} with high selectivity (GaAs : resist = 30 : 1) were obtained. Damage to the wafers was low. However micro-loading and sidewall bowing were

observed. Chen and Yang [25] used a grid to extract positive ions out of an ICP source. A second grid was used to neutralize these ions before etching a wafer downstream. They realized high rate (600 nm min^{-1}) anisotropic etching of polymer films. High rate (~500 nm min^{-1} at room temperature) polymer etching using an oxygen neutral beam was also obtained in [26, 27]. Microloading-free, high aspect ratio (5 : 1) etching of 0.25 μm wide features with straight sidewalls was demonstrated. Sidewall bowing and undercut typically seen in plasma or RIE of polymers were completely absent. The etch rate was independent of the substrate temperature (up to 85 °C) indicating that etching was due to fast neutrals as opposed to thermal energy neutrals.

Samukawa and co-workers [28, 29, 49–51] used F-atom and Cl-atom containing fast neutral beams to etch polysilicon gates. The neutral beams were generated in F_2 or SF_6 and Cl_2 plasmas, respectively. The SF_6 based neutral beam resulted in a silicon undercut because of the generation of a large concentration of F radicals. The Cl_2 based neutral beam showed no undercut and very high selectivity (100 : 1) over the underlying oxide, but the etch rate was very low (4.3 nm min^{-1}). The F_2 based neutral beam provided a compromise with an etch rate of 29.4 nm min^{-1}, albeit with reduced selectivity over oxide [49]. To examine the charging damage, the authors etched polysilicon gates. The gate oxide thickness was reported to be about 5 nm. The leakage current of MOS capacitors fabricated using a neutral beam was about an order of magnitude lower than those fabricated using conventional RIE [49]. Neutral beam etching (NBE) was also found to be superior to conventional plasma processing when fabricating fin FETs (field effect transistors) with vertical Si fins [50]. Specifically, the electron mobility in the channel was larger for the neutral beam processed samples. It was speculated that exposure to VUV and UV radiation during plasma processing created surface roughness that reduced electron mobility. Such radiation was effectively blocked in NBE.

Kubota *et al* [51] used a neutral beam to pattern sub 10 nm diameter structures. Ferritin (a protein) with a 7 nm diameter iron core was dispersed on a silicon substrate. After removing the protein shell, the iron core served as a hard mask to etch the exposed silicon and create sub 10 nm diameter silicon nano-columns with an aspect ratio (height to diameter) of ~5 : 1. A low energy (~10 eV) chlorine neutral beam was used for etching. High resolution TEM pictures showed that the neutral beam did not introduce damage in the silicon lattice. RIE using a chlorine ECR plasma resulted in very low selectivity of the iron mask compared with silicon, and high aspect ratio silicon nano-columns could not be fabricated. The authors attributed the differences between RIE and NBE mainly to VUV and UV photons emanating from the plasma. Such photons are effectively blocked in the case of NBE. However, there was no convincing evidence that photons played a significant role, and the energy distributions of bombarding ions (in RIE) and fast neutrals (in NBE) were not measured.

Integration of porous low-k materials for interconnect technology presents many challenges to the etch, ash and clean processes. One challenge is the post etch removal of photoresist over porous low-k films. Porous low-k films are very susceptible to damage by plasma processing, which can raise the overall effective dielectric constant k_{eff} of the film. A pure oxygen plasma ash cannot be used because chemical and physical damage occurs. In contrast, a pure oxygen fast neutral beam can ash photoresist over porous low-k dielectrics without damaging the exposed low-k material [27, 52]. H_2 or H_2/N_2 neutral beam ashing apparently results in the formation of a dense surface layer ('crust') on a porous methyl-silsesquioxane porous dielectric (MSQ, dielectric constant of 2.2) which protects the inner film from damage [52].

Neutral beams with much lower (<10 eV) energy have also been reported. Giapis *et al* [53], using a laser detonation technique, obtained a F-atom beam with a flux of 2×10^{14} atoms cm^{-2} s^{-1} and energy less than 10 eV. The ion fraction was less than 1%. An etch rate of 30 nm min^{-1} for Si with 14% undercutting was obtained. Campos *et al* [54] used laser vaporization of a cryogenic Cl_2 film to generate a hyperthermal (maximum energy 6 eV) molecular beam. The etch rate of Si with the neutral beam was greater than that with thermal chlorine by a factor >30. Using a hyperthermal beam (~1 eV) of molecular chlorine produced by free jet expansion of a Cl_2 gas heated in a graphite furnace, Suzuki *et al* [55] obtained highly anisotropic etching of poly-Si with an etch rate of 3.1 nm min^{-1}. Selectivity over SiO_2 was more than 1000. C–V studies showed that the damage levels were much lower than those by plasma or ion beam processes. Using the same technique to produce hyperthermal Cl_2, Ono *et al* [56] etched GaAs at 1.5 μm min^{-1}. Larson *et al* [57] etched 1 μm wide high aspect ratio trenches (120 : 1) in silicon using a 1 eV neutral atomic fluorine beam with a rate of 1.2 μm min^{-1} at 500 °C without ARDE. This incredible aspect ratio could apparently be achieved by using a highly collimated beam. Some kind of 'wave-guiding' effect might be taking place in the deep trench, whereby fast atoms suffer grazing angle collisions with the sidewalls of the trench and are 'guided' to the bottom of the trench where etching takes place. Apparently fast F-atoms do not react with the sidewall even at 500 °C when they collide at grazing angles.

To achieve uniform etching (or deposition) using a fast neutral beam, the beam flux must be uniform across the wafer radius. This implies that the parent ion beam must also be uniform. Uniform ion beams over large area substrates have been demonstrated [78]. Ways to control the ion (and thus neutral) beam energy are also available (see [79] and references therein). Neutral beams formed by ion extraction and neutralization through high aspect ratio holes have an inherent anisotropy determined, in part, by the aspect ratio of the holes.

3.2. Atomic layer etching

The atomic layer etching (ALET) concept is demonstrated schematically in figure 6, which shows a complete cycle of the process [58, 59]. The cycle consists of the following four steps.

1. Exposure of a clean surface to a gas and adsorption (chemisorption) of the gas onto the surface.

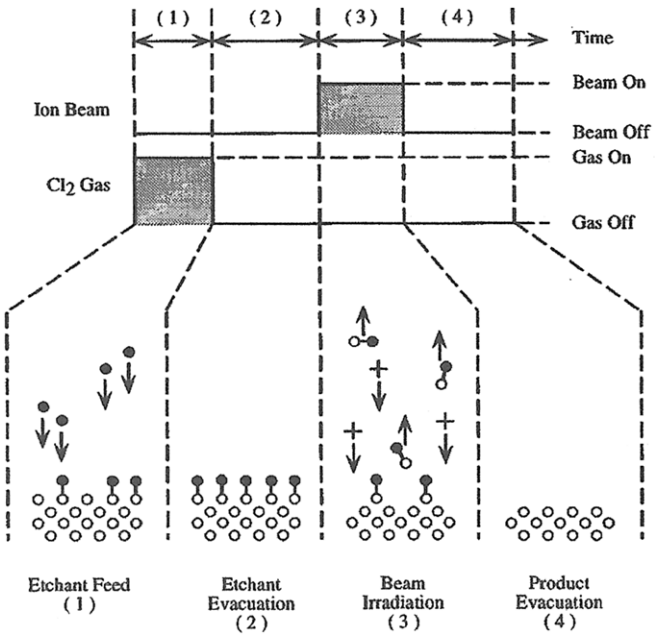

Figure 6. The four steps of ALET: etchant feed to form a monolayer of adsorbed gas, excess etchant evacuation, beam irradiation to remove the top layer of the solid and product evacuation. (From [58].)

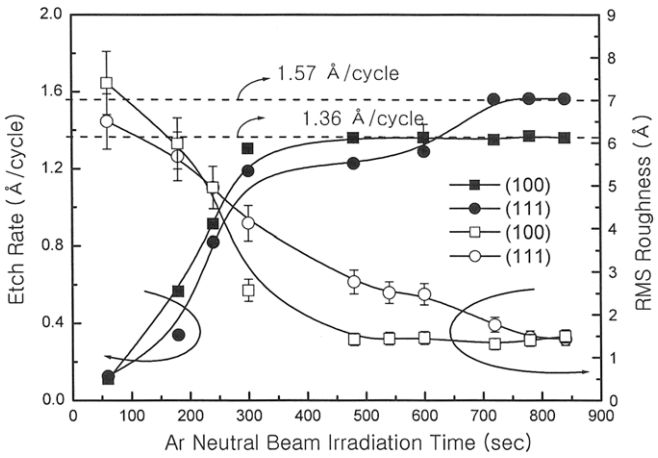

Figure 7. ALET of silicon using a neutral beam source. The etch rate (in Å per cycle) and the surface roughness are shown as a function of the Ar neutral beam irradiation time in step 3. For given beam flux, the beam irradiation time corresponds to beam dose. (From [60].)

2. Evacuation of the chamber so that only the chemisorbed layer can subsequently react. This step is necessary to avoid etching by gas phase species in the subsequent step.
3. Exposure to an energetic beam to effect chemical reaction between the adsorbed gas and the underlying solid. Ideally, exactly one monolayer of the solid is removed in this step.
4. Evacuation of the chamber to exhaust the reaction products.

Completion of a cycle results, hopefully, in the etching of one atomic layer of the film. The cycle can be repeated to etch as many atomic layers as required. Etching with monolayer accuracy places some limitations regarding the choice of gas and energetic beam. For example, the gas must be selected such that spontaneous etching of the solid does not occur in step 1. This may not a severe limitation since, even if spontaneous etching would normally occur, cooling of the substrate at sufficiently low temperature would quench the spontaneous reaction, without affecting the reaction in step 3 (in step 3, energy is supplied by the energetic beam, i.e. this is not a thermally activated process). Also, the energetic beam must be chosen so that the process is self-limiting, i.e. once surface reaction has been completed in step 3, any further irradiation by the energetic beam should not damage the exposed underlayer. This implies, for example, that the beam energy should be below the (physical) sputtering threshold. If the above precautions are not taken, etching with monolayer accuracy is not possible.

Park *et al* [60] demonstrated ALET of single crystal silicon with chlorine (figure 7). They used an Ar neutral beam with ~50 eV energy for step 3. When the chlorine dose in step 1 and/or the neutral beam dose in step 3 were below a critical value, the etch rate (Å/cycle) and the surface roughness varied with the dose. When both the chlorine gas dose and the neutral beam dose were above a critical value, the saturated etch rate of one monolayer per cycle (1.36 Å/cycle for Si (1 0 0) and 1.57 Å/cycle for Si(1 1 1)) resulted. Under these conditions, the surface roughness of the etched sample was 1.45 Å, similar to the starting sample before etching. It appears that for doses above their critical values, the silicon surface was covered by a monolayer of chlorine in step 1 and this monolayer was removed as silicon chloride upon exposure to the neutral beam in step 3. Surface coverage by chlorine in step 1 and removal of silicon species by the neutral beam in step 3 was self-limiting. Park *et al* [61] also demonstrated ALET of InP using chlorine and a Ne neutral beam.

ALET requires a tight control of ion (or neutral beam) energy. Normally, a broad energy distribution is obtained with an ion source [74, 80]. A method to obtain a nearly monoenergetic beam is reported in [79] (see also references therein).

3.3. Thin film deposition

Lu and co-workers [23, 24] used a neutral beam of nitrogen simultaneously with electron beam evaporation of boron to deposit mostly (80%) cubic phase, stoichiometric boron nitride (c-BN) films on silicon substrates, at the relatively low temperature of 400–500 °C. A Kaufman-type ion source was used to obtain an ion beam that was neutralized by a conical surface, which also acted as a 'funnel' to focus the resulting neutral beam on the substrate surface. The films were compared with those obtained under similar conditions but without neutralizing the nitrogen beam. It was found that the c-BN content of the grown films was reduced drastically (to 10%). It was concluded that the neutral beam was a critical factor in enhancing the formation of c-BN. The electrical characteristics of BN films doped with Mg were also reported [24]. Atom beam modification of insulator surfaces was studied in [22]. Mueller *et al* [62] grew crystalline GaN

films on bare *c*-axis-oriented sapphire at very low temperatures (100–500 °C). A collimated beam of N atoms (kinetic energy 0.5–5 eV) was created by the expansion of a laser-generated plasma through a supersonic nozzle. A flux of Ga metal was simultaneously supplied to the substrate by electron beam evaporation. The GaN film growth rate was ∼0.5–2 μm h^{-1} and was limited by the Ga supply. Samukawa *et al* [63] used a nitrogen neutral beam in a pulsed mode to control the dose and spatial distribution of nitrogen in a 2 nm thick silicon dioxide film in an effort to form oxynitride gate dielectrics.

3.4. Neutral beam lithography

Neutral beam lithography (NBL) is essentially identical to ion proximity printing [64] except that a neutral beam is used instead of an ion beam [65]. A helium ion or proton beam (kinetic energy of tens of keV) is neutralized by passing the beam through a charge exchange cell (volume neutralization). A differentially pumped drift region is used to collimate the resulting neutral beam. An ion sensitive resist on the substrate is exposed through a stencil mask in close proximity to the substrate. The use of a neutral beam can provide finer nanostructures compared with an equivalent ion beam, since beam deflection due to charging is not an issue with neutrals.

Film deposition and lithography by manipulating atom beams using laser light or magnetic forces has been reviewed by Meschede and Metcalf [66]. For example, metastable atom beams can be localized with optical standing waves [67] and used for lithography. Although interesting from the scientific point of view, these techniques have less chance of being used in manufacturing.

3.5. Neutral beams in fusion plasmas

High energy (tens to hundreds of keV) neutral beams are used to heat controlled nuclear fusion plasmas under magnetic confinement [68, 69]. Negative ion beams are preferred because they can be neutralized more efficiently at energies greater than ∼50 keV [69]. A common negative ion source is that using hydrogen gas for the production of negative H^- ions [70,71]. These ions are eventually accelerated and neutralized before being injected in the fusion reactor. To produce H^-, a pulsed plasma in hydrogen gas may be used. Highly excited vibrational states of molecular hydrogen formed in the active glow (when plasma power is on) attach cold electrons in the afterglow (when plasma power is off) to form negative ions. These ions are extracted by the application of a bias through an aperture at the reactor wall. The presence of a weak magnetic field can modify the structure of the potential field close to the extraction hole of the negative ion source, thereby enhancing the extracted negative ion flux [72]. Heavy-ion (Cl^-) fusion drivers for inertial confinement have also been studied [68], where chlorine ions were extracted from an essentialy ion–ion plasma.

4. Neutral beam diagnostics

Neutral beam diagnostics are important to measure the flux, energy distribution and angular distribution (collimation) of the beam. In contrast to ion beams, neutral beam characterization is not as easy, since neutrals cannot be manipulated with electric (or magnetic) fields. Neutral beam diagnostics fall into two general categories: measure the properties of the neutrals directly or first ionize (a part of) the neutral beam and then characterize the resulting ions. Calorimetry may be used to directly measure the energy flux of a neutral beam [28, 29, 75, 81]. The temperature rise as a function of time of the calorimeter disc is related to the power deposited on the calorimeter. Care must be exercised to exclude ions, electrons or photons reaching the calorimeter. Even then, however, calorimetry provides the energy flux (i.e. particle flux times energy), and not the individual values of the neutral beam flux and energy. A common approach is to assume that the neutral beam energy distribution is the same as the energy distribution of residual ions coming out of the source [20,29,49,52], which can be readily obtained with a gridded electrostatic ion energy analyzer. The neutral beam flux can then be extracted. Even if the energy distribution of the neutral beam is accurately known, however, calorimetry provides only an approximate measure of the neutral beam flux, since the fraction of energy that neutrals actually deposit when they strike the calorimeter surface is generally unknown [73]. It is usually assumed that all of the energy of the bombarding species is deposited on the surface. Another method to measure the neutral beam flux makes use of the secondary electron current emitted from a surface impacted by fast neutrals [20, 29]. Again, ions, electrons and photons must be excluded from striking the detector surface or their effect accounted for. Even then, however, one must know the secondary electron emission coefficient, γ, of the surface as a function of energy for the particular fast neutrals. Also, the detector surface must be kept 'clean' otherwise γ may be a function of source operating conditions.

The energy distribution of a fast neutral beam may be measured by ionizing a fraction of the beam (for example using a crossed electron beam) and measuring the resulting ion energy distribution (IED) [13, 25, 74, 75]. A simple correction must be applied based on the fact that the 'contact time' of neutrals with the electron beam depends on the neutral kinetic energy. The ionized neutrals are detected using time of flight (TOF) or lock-in amplification techniques.

The energy distribution and flux of fast neutrals and residual ions extracted from a neutral beam source were measured by Ranjan and co-workers [74, 75], using an electrostatic energy analyzer. The fast neutral energy distribution (NED) was always shifted to lower energies (figure 8) compared with the corresponding residual IED. This reflects the energy loss in collisions of ions with the sidewall of the grid holes (equation (2)). The NE, defined as the ratio of the fast neutral flux to the total (residual ion plus fast neutral) flux, increased with plasma power and decreased with boundary voltage. The residual ion current decreased monotonically with increasing hole diameter and hole aspect ratio. Larger holes result in more severe plasma moulding (figure 3) and more ions are diverted to strike the sidewall of the grid holes and neutralize.

To ascertain the effect of surface roughness of the neutralization grid, the energy distribution and flux of fast

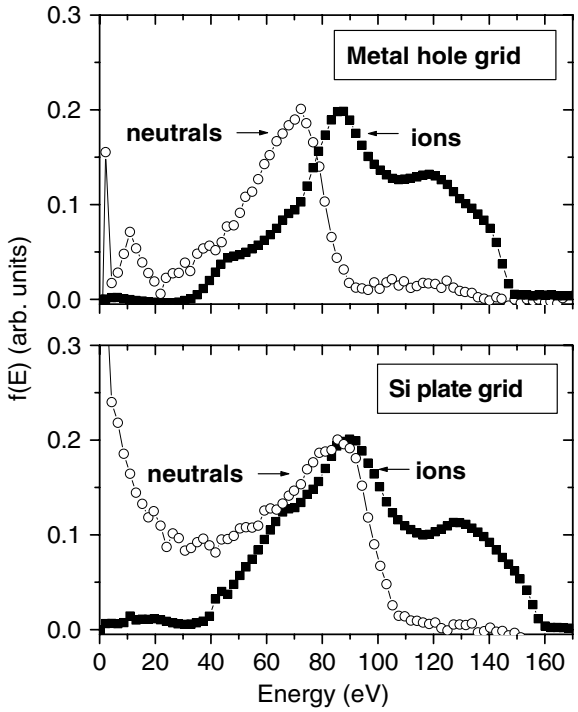

Figure 8. Residual IEDs and fast NEDs extracted from a neutral beam source with a metal hole grid (top) and a silicon plate grid (bottom). Conditions: 150 W plasma power, 10 mTorr pressure and 50 V boundary voltage. (From [75].)

neutrals and residual ions extracted from the neutral beam source were measured using two different neutralization grids: one with relatively rough internal surface of holes drilled through an aluminium disc (metal hole grid) and one with atomically smooth parallel surfaces (Si plate grid) made from pieces of thinned, double-side polished Si wafers [75]. Energy distributions measured for a 150 W, 10 mTorr plasma with a boundary voltage $V_b = 50$ V are shown in figure 8. The residual IEDs for the two grids (solid squares) are nearly the same. This reflects the fact that residual ions exiting the grid do not collide with the surface and, therefore, the surface roughness is immaterial. In contrast, the NEDs for the two grids are quite different. The peak in the NED, relative to the IED, is 3 eV lower for the Si plate grid and 14 eV lower for the metal hole grid. In addition, the population of low energy neutrals (below 50 eV) is considerably higher with the Si grid. Ions near the peak of the IED undergoing glancing angle collisions with the smooth Si grid are much more likely to scatter specularly and lose little energy compared with those scattered from the rough metal grid surfaces. For the same reason, neutrals are more likely to make several bounces off the smooth, parallel Si grid surfaces and emerge as lower energy (<50 eV) neutrals with relatively low angular spread. The residual ion flux and fast neutral flux were observed to be 2 to 4 times higher for the Si grid than for the metal grid [75]. The higher transparency of the Si grid could explain, in part, the higher fluxes. The smoothness of the Si surface and resulting specular reflection could explain the additional fast neutral flux. The NE with the Si grid was between about 50 and 90%.

In principle, the energy distribution of a fast neutral beam may also be measured by exciting neutrals using an electron beam and observing the Doppler shift of the light emission emanating from the fast neutrals. A high resolution spectrometer is needed to differentiate the wavelength shifted signal from the (normally much larger) emission of the background thermal energy atoms. In practice, this technique should work for fast neutrals with high enough energy so that the Doppler shifted signal is not 'buried' under the 'wing' of the thermal energy neutral emission peak. The author is not aware of any reports using this technique to characterize fast neutral beams of interest in this paper.

Measurements of the angular distribution of fast neutral beams have not been reported. An indirect measurement was performed by Yunogami *et al* [13] who measured the angular divergence of the residual ions emanating from the neutral beam source. Also, a rough idea of the beam divergence may be obtained by measuring the etch rate drop off as a function of distance from the neutralization grid [26] or by using techniques applied to ion beams [82]. In principle, the fast neutral beam may be ionized (using an electron beam) and the ion current measured as a function of (angular) position. However, the resulting current may be too small to provide an adequate signal-to-noise ratio.

5. Concluding remarks

Fast (kinetic energy of tens to hundreds of eV) neutral beams may be beneficial in situations where conventional plasma processing can introduce damage due to charging or VUV/UV radiation [76]. Neutral beam sources can deliver the flux and anisotropy required for several applications, for example, polymer etching. A practical application may be bilayer resist, where the neutral beam is used to etch the bottom polymer layer. RIE may introduce sidewall bow and undercut which are absent in neutral beam etching.

It appears that even pure oxygen neutral beams may be suitable for photoresist ashing over low-k dielectrics. This is probably because NBE is due to directional fast neutrals that react with high probability at the feature bottom and do not introduce sidewall damage to the porous low-k film. It should be noted that the thermal neutral flux striking the wafer is very low, since the pressure over the wafer is typically <0.5 mTorr. High rate silicon dioxide NBE has not been demonstrated. The low flux of thermal energy neutrals may be the culprit, since conventional oxide etching is ion induced but (thermal) neutral controlled [77]. NBE may have a particular advantage in ALET of insulating materials. Being a 'gentler' process (no charging, very little VUV/UV radiation) compared with RIE, NBE may also be superior in the etching of ultra thin (∼tens of nm) films, for which the possibly lower etch rate of NBE has no significant throughput consequences. Large area (300 mm diameter or more) neutral beam processing has not been demonstrated yet, but appears feasible given the viability of large area ion beam sources [78]. From the practical point of view, pumping requirements are expected to be demanding for large wafer processing. Also, large diameter grids must have provisions for adequate heat transfer to avoid warping of the grid.

Low kinetic energy (<10 eV) neutral beam sources have also demonstrated high rate anisotropic etching. For example, Larson *et al* [57] etched 1 μm wide high aspect ratio trenches (120 : 1) in silicon using a 1 eV neutral atomic fluorine beam at a rate of 1.2 μm min^{-1} at 500 °C. However, large area uniformity is a serious issue with such sources.

Acknowledgments

The author is grateful to the State of Texas (Texas Advanced Technology and Texas Advanced Research Programs) and the National Science Foundation (MRI-0521523) for financial support of this work. Early financial support by an ISSO grant and a GEAR grant of the University of Houston is also gratefully acknowledged. The author would like to thank Professor Vincent Donnelly (University of Houston), Dr Lee Chen (Tokyo Electron America) and Professor Seiji Samukawa (Tohoku University, Japan) for fruitful discussions.

References

[1] Lieberman M A and Lichtenberg A J 2005 *Principles of Plasma Discharges and Materials Processing* 2nd edn (New York: Wiley)
[2] Economou D J and Alkire R C 1988 *J. Electrochem. Soc.* **135** 941
[3] Arnold J C and Sawin H H 1991 *J. Appl. Phys.* **70** 5314
[4] Fujiwara N, Maruyama T and Yoneda M 1996 *Japan. J. Appl. Phys.* **35** 2450
[5] Matsui J, Nakano N, Petrovic Z Lj and Makabe T 2001 *Appl. Phys. Lett.* **78** 883
[6] Gottscho R A, Jurgensen C W and Vitkavage D J 1992 *J. Vac. Sci. Technol.* B **10**
[7] Hwang G S and Giapis K P 1997 *J. Vac. Sci. Technol.* B **15** 70–87
[8] Kinoshita T, Hane M and McVittie J P 1996 *J. Vac. Sci. Technol.* B **14** 560–5
[9] Gabriel C T and McVittie J P 1992 *Solid State Technol.* **35** 81–7
[10] Leone S R 1995 *Japan. J. Appl. Phys.* **34** Part 1 2073–82
[11] Caledonia G E, Krech R H and Oakes D B 1996 *J. Inst. Environ. Sci.* 23–8 March/April
[12] Mizutani T and Yunogami T 1990 *Japan. J. Appl. Phys.* **29** 2220
[13] Yunogami T, Yogokawa K and Mizutani T 1995 *J. Vac. Sci. Technol.* A **13** 952
[14] Yokogawa K, Yunigami T and Mizutani T 1996 *Japan. J. Appl. Phys.* **35** 1901
[15] Tsuchizawa T, Jin Y and Matsuo S 1994 *Japan. J. Appl. Phys.* **33** 2200
[16] Jin Y, Tsuchizawa T and Matsuo S 1995 *Japan. J. Appl. Phys.* **34** L465
[17] Goeckner M J, Bennett T K and Cohen S A 1997 *Appl. Phys. Lett* **71** 980
[18] Shimokawa F, Tanaka H, Uenishi Y and Sawada R 1989 *J. Appl. Phys.* **66** 2613
Shimokawa F 1992 *J. Vac. Sci. Technol.* A **10** 1352
[19] Kuwano H and Shimokawa F 1988 *J. Vac. Sci. Technol.* B **6** 1565
[20] Kim S J, Wang S J, Lee J K, Lee D H and Yeom G Y 2004 *J. Vac. Sci. Technol.* A 1948–55
[21] Nichols C A and Manos D M 1996 *J. Appl. Phys.* **80** 2643
[22] Eipers-Smith K, Waters K and Schultz J A 1993 *J. Am. Ceram. Soc.* **76** 284
[23] Lu M, Bousetta A, Sukach R, Bensaoula A, Waters K, Eipers-Smith K and Schultz J A 1994 *Appl. Phys. Lett.* **64** 1514–16
[24] Lu M, Bousetta A, Bensaoula A, Waters K and Schultz J A 1996 *Appl. Phys. Lett.* **68** 622–4
[25] Chen L and Yang Q 1996 *Electrochemical Soc. Proc. (Los Angeles, CA)* vol 96–12, ed G S Mathad and M Meyyappan p 332
[26] Panda S, Economou D J and Chen L 2001 *J. Vac. Sci. Technol.* A **19** 398–404
[27] White B, Wang Q, Economou D J, Wolf P J, Jacobs T and Fourcher J 2003 *Proc. IEEE Int. Interconnect Technology Conf. (San Francisco, 2–4 June 2003)* p 153
[28] Samukawa S, Sakamoto K and Ichiki K 2001 *Japan. J. Appl. Phys.* **40** Part 2 L779–82
[29] Samukawa S, Sakamoto K and Ichiki K 2002 *J. Vac. Sci. Technol.* A **20** 1566–73
[30] Kim D and Economou D J 2002 *IEEE Trans. Plasma Sci.* **30** 2048–58
[31] Helmer B A and Graves D B 1998 *J. Vac. Sci. Technol.* A **16** 3502
[32] Hwang G S, Anderson C M, Gordon M J, Moore T A, Minton T K and Giapis K P 1996 *Phys. Rev. Lett.* **77** 3049
[33] Hagstrum H D 1954 *Phys. Rev.* **96** 336
[34] Hagstrum H D 1961 *Phys. Rev.* **122** 83
[35] Hagstrum H D 1966 *Phys. Rev.* **150** 495
[36] Rabalais J W, Chen J-N, Kumar R and Narayana N 1985 *J. Chem Phys.* **83** 6489
[37] Hird B, Gauthier P, Bulicz J and Armstrong R A 1991 *Phys. Rev. Lett.* **67** 3575
[38] Brako R and Newns D M 1981 *Surf. Sci.* **108** 253
[39] Kang H, Kasi S R and Rabalais J W 1988 *J. Chem. Phys.* **88** 5882
Kang H, Kasi S R, Grizzi O and Rabalais J W 1988 *J. Chem. Phys.* **88** 5894
Kasi S R, Kilburn M A, Kang H, Rabalais J W, Tavernini L and Hochmann P 1988 *J. Chem. Phys.* **88** 5902
Kasi S R, Kang H and Rabalais J W 1988 *J. Chem. Phys.* **88** 5914
[40] Kaganovich I D, Ramamurthi B N and Economou D J 2001 *Phys. Rev.* E **64** 036402
[41] Economou D 2007 *Appl. Surf. Sci.* **253** 6672–80
[42] Abolmasov S N, Ozaki T and Samukawa S 2007 *J. Vac. Sci. Technol.* A **25** 134–40
[43] Yonekura K, Goto K, Matsuura M, Fujiwara N and Tsujimoto K 2005 *Japan. J. Appl. Phys.* **44** 2976
[44] Kim D, Economou D J, Woodworth J R, Miller P A, Shul R J, Abraham I C, Aragon B P and Hamilton T W 2003 *IEEE Trans. Plasma Sci.* **31** 691–702
[45] Woodworth J R, Miller P A, Shul R J, Abraham I C, Aragon B P, Hamilton T W, Willison C G, Kim D and Economou D J 2003 *J. Vac. Sci. Technol.* A **21** 147–55
Kim D and Economou D J 2002 *IEEE Trans. Plasma Sci.* **30** 2048–58
[46] Kim C-K and Economou D J 2002 *J. Appl. Phys.* **91** 2594–603
[47] Nam S K, Economou D J and Donnelly V M 2007 *Plasma Sources Sci. Technol.* **16** 90–6
Nam S K, Economou D J and Donnelly V M 2006 *J. Phys. D: Appl. Phys.* **39** 3994–4000
[48] Nam S K, Economou D J and Donnelly V M 2007 *IEEE Trans. Plasma Sci.* at press
[49] Noda S, Nishimori H, Iida T, Arikado T, Ichiki K, Ozaki T and Samukawa S 2004 *J. Vac. Sci. Technol.* A **22** 1506
Noda S, Ozaki T and Samukawa S 2006 *J. Vac. Sci. Technol.* A **24** 1414–20
[50] Samukawa S and Endo K 2007 Ultimate top–down etching processes for future nanoscale devices *Proc. 8th Int. Conf. on Solid-State and Integrated Circuit Technology (ICSICT-2006, Shanghai, China)* pp 462–5

[51] Kubota T, Baba T, Samukawa S, Kawashima H, Uraoka Y, Fuyuki T and Yamashita I 2004 *Appl. Phys. Lett.* **84** 1555
[52] Ohtake H, Inoue N, Ozaki T, Samukawa S, Soda E and Inukai K 2005 *J. Vac. Sci. Technol.* B **23** 210–16
[53] Giapis K P, Moore T A and Minton T K 1995 *J. Vac. Sci. Technol.* A **13** 959
[54] Campos F X, Weaver G C, Waltman C J and Leone S R 1992 *J. Vac. Sci. Technol.* B **10** 2217
[55] Suzuki K, Hiraoka S and Nishimatsu S 1988 *J. Appl. Phys.* **64** 3697
[56] Ono T, Kashima H, Hiraoka S, Suzuki K and Jahnke A 1991 *J. Vac. Sci. Technol.* B **9** 2978
[57] Larson P R, Copeland K A, Dharmasena G, Lasell R A, Keil M and Jonhson M B 2000 *J. Vac. Sci. Technol.* B **18** 307–12
[58] Athavale S D and Economou D J 1995 *J. Vac. Sci. Technol.* A **13** 966–71
[59] Athavale S D and Economou D J 1996 *J. Vac. Sci. Technol.* B **14** 3702
[60] Park S D, Oh C K, Lee D H and Yeom G Y 2005 *Electrochem. Solid State Lett.* **8** C177–9
[61] Park S D, Oh C K, Bae J W, Yeom G Y, Kim T W, Song J I and Jang J H 2006 *Appl. Phys. Lett.* **89** 043109-1–043109-3
[62] Mueller A H, Akhadov E A and Hoffbauer M A 2006 *Appl. Phys. Lett.* **88** 041907-1–041907-3
[63] Samukawa S, Minemura Y and Fukuda S 2004 *J. Vac. Sci. Technol.* A **22** 249
[64] Ruchhoeft P, Wolfe J C and Bass R 2001 *J. Vac. Sci. Technol.* B **19** 2529–32
[65] Wolfe J C and Craver B P 2008 *J. Phys. D: Appl. Phys.* **41** 024007 (this issue)
[66] Meschede D and Metcalf H 2003 *J. Phys. D: Appl. Phys.* **36** R17–38
[67] Johnson K S, Thywissen J H, Dekker N H, Berggren K K, Chu A P, Younkin R and Prentiss M 1998 *Science* **280** 1583–6
[68] Grisham L R, Kwan J W, Hahto S K, Hahto S T, Leung K N and Westenskow G 2006 *Rev. Sci. Instrum.* **77** 03A501-1–03A501-6
[69] Hemsworth R S and Inoue T 2005 *IEEE Trans. Plasma Sci.* **33** 1799–813
[70] Hass F A, Lea L M and Holmes A J T 1991 *J. Phys. D: Appl. Phys.* **24** 1541
[71] Bacal M, Hatayama A and Peters J 2005 *IEEE Trans. Plasma Sci.* **33** 1845
[72] Hatayama A, Matsumiya T, Sakurabayashi T and Bacal M 2006 *Rev. Sci. Instrum.* **77** 1
[73] Winters H, Coufal H, Rettner C T and Bethune D S 1990 *Phys. Rev.* B **41** 6240–56
[74] Ranjan A, Donnelly V M and Economou D J 2006 *J. Vac. Sci. Technol.* A **24** 1839–46
[75] Ranjan A, Helmbrecht C, Donnelly V M, Economou D J and Franz G 2007 *J. Vac. Sci. Technol.* B **25** 258–63
[76] Samukawa S 2006 *Japan. J. Appl. Phys.* **45** 2395–407
[77] Feldsien J, Kim D and Economou D J 2000 *Thin Solid Films* **374** 311–25
[78] Kanarov V, Hayes A, Yevtukhov R, Kameyama I, Siegfried D and Wahlin E 2006 *Rev. Sci. Instrum.* **77** 03B515
[79] Xu L, Economou D J, Donnelly V M and Ruchhoeft P 2005 *Appl. Phys. Lett.* **87** 041502
[80] Zeuner M, Meichsner J, Neumann H, Scholze F and Bigl F 1996 *J. Appl. Phys.* **80** 611
[81] Kersten H, Deutsch H, Steffen H, Kroesen W G M and Hippler R 2001 *Vacuum* **63** 385–431
[82] Kahn J R, Kaufman H R, Phillips C A and Robinson R S 1996 *J. Vac. Sci. Technol.* A **14** 2106–112